ATLAS NOTE

November 13, 2009

Expected performance of the ATLAS detector in GMSB models with τ final states

The ATLAS Collaboration

ATL-PHYS-PUB-2009-089
13 November 2009

Abstract

Gauge Mediated Supersymmetry Breaking (GMSB) models provide a possible mechanism to mediate supersymmetry to the visible sector. In these models the lightest supersymmetric particle is usually the gravitino, while the next-to-lightest supersymmetric particle (NLSP) is either a neutralino or a slepton. In the case of a $\widetilde{\tau}$ NLSP, events with large missing transverse energy, highly energetic jets and up to four tau leptons are expected in pp-collisions at the LHC providing a powerful channel to probe the GMSB theory.

In this note we study the expected performance of the ATLAS detector in GMSB scenarios with a $\widetilde{\tau}$ NLSP for a LHC centre-of-mass energy of $\sqrt{s} = 10\,\text{TeV}$. A cut-based selection is optimised using an example GMSB signal and a scan of the GMSB parameter space is performed to determine the discovery reach as a function of the integrated luminosity. In addition, the invariant mass distribution of two tau leptons is used to study the measurement of masses of supersymmetric particles with larger event samples.

1 Introduction

The main goals of the two multi-purpose experiments ATLAS [1] and CMS [2] at the LHC [3] are the study of electroweak symmetry breaking and the search for physics beyond the Standard Model (SM). Among the many proposed extensions of the SM, Supersymmetry (SUSY) [4–7] is considered a key candidate because it solves several shortcomings of the SM in an elegant way. For example, SUSY may provide a dark matter candidate and allows the unification of the coupling constants at a GUT scale. Since supersymmetric particles should have the same mass as their superpartners but have not yet been observed, SUSY is a broken symmetry. However, the breaking mechanism is unknown . It is usually assumed that the breaking takes place at a high energy scale and SUSY is then mediated to the visible sector via mechanisms such as gravity mediation, gauge mediation or anomaly mediation. The mass spectrum of the SUSY particles and the phenomenology are largely determined by the mediation mechanism, in particular by the nature of the lightest supersymmetric particle (LSP) which is stable if R-parity is assumed to be conserved.

With the high luminosity and the high centre-of-mass energy of the proton-proton-collisions available at the LHC, squarks and gluinos are assumed to be produced copiously via the strong interaction for many SUSY models. In the past, the ATLAS and CMS collaborations have focused their studies [8,9] on minimal Super Gravity (mSUGRA) models [10–14] where the LSP is usually the lightest (but massive) neutralino, leading to final states characterised by multiple highly energetic jets and large missing transverse energy (E_T^{miss}). In contrast, Gauge Mediated Supersymmetry Breaking (GMSB) models [15–21] feature a gravitino ($\widetilde{G}$) LSP which is neutral and almost massless. In these models the next-to-lightest supersymmetric particle (NLSP) is either the lightest neutralino $\widetilde{\chi}_1^0$, the lightest stau ($\widetilde{\tau}_1$) or a right-handed slepton ($\widetilde{\mathrm{e}}_R, \widetilde{\mu}_R$) leading to final states containing photons, τ leptons or leptons (e and μ), respectively. While the ATLAS performance in GMSB scenarios with final state photons has been studied in [8] (p.1660), we study here the case of a prompt decaying $\widetilde{\tau}_1$ NLSP with τ leptons in the final state.

In this study the ATLAS discovery potential in the GMSB parameter space with τ final states is determined for a centre-of-mass energy of $\sqrt{s} = 10\,\mathrm{TeV}$ using a cut-based analysis applied to simulated event samples. For a characteristic GMSB benchmark scenario in which a large amount of E_T^{miss} (from the escaping $\widetilde{G}$ LSP), highly energetic jets (from the initial squark/gluino decays) and a large number of τ leptons (from the $\widetilde{\tau}_1$ NLSP decay) are expected, the event selection is optimised using signal and background samples simulated with a full GEANT4-based [22, 23] detector response. The event selection is then applied to simulated event samples of various other GMSB scenarios in a scan of the GMSB parameter space. The corresponding data samples have been simulated using a fast simulation approach [24] after a careful comparison of the fast and full simulation results. In addition, we study the prospects for the measurement of endpoints in the invariant mass spectra of two τ leptons in the final state for the above-mentioned GMSB benchmark scenario.

The discovery potential has been studied for $\sqrt{s} = 10\,\mathrm{TeV}$ which is the centre-of-mass energy for which $200\,\mathrm{pb}^{-1}$ are expected in the early phase of the LHC. Simulated events corresponding to $8\,\mathrm{fb}^{-1}$ with the same centre-of-mass energy have been used in the study of the invariant di-tau mass distribution to illustrate the technique for the determination of kinematic end-points. This technique is foreseen to be applied to the large data samples expected to be recorded at the nominal LHC centre-of-mass energy of $\sqrt{s} = 14\,\mathrm{TeV}$.

This note is organised as follows. The next section gives a short description of the GMSB models, the relevant parameters and the phenomenology expected at the LHC. An overview of the event simulation and the samples used in this study is given in Section 3 together with a

comparison of fast and full simulation results. The optimisation of the signal selection and the investigation of the ATLAS discovery potential in the GMSB parameter space is discussed in Section 4. Finally, the study of SUSY mass measurements from the invariant mass distribution of two τ leptons is presented in Section 5.

2 GMSB models

In GMSB models [15–21] Supersymmetry is communicated from the hidden sector to the visible sector through a flavor-blind SM gauge interaction via messenger fields at a scale M_m which is small compared to the Planck mass. In the minimal GMSB model the messenger fields form complete representations of $SU(5)$ and therefore preserve the unification of the coupling constants. Squarks, sleptons and gauginos obtain their masses radiatively from the gauge interactions with the massive messenger fields in such a way that the superpartner masses are proportional to the breaking scale. The free parameters in GMSB models are the following:

- Λ: the scale of the SUSY breaking; typically it has values of $(10 - 100)$ TeV and sets the overall mass scale for all MSSM superpartners, which depend linearly on Λ.
- M_m: the messenger mass scale; it has to be larger than Λ in order to prevent color and charge breaking in the messenger sector.
- N_5: the number of equivalent messenger fields; the gaugino masses depend linearly on N_5 while the sfermion masses are proportional to $\sqrt{N_5}$.
- $\tan\beta$: the ratio of the two Higgs doublet vacuum expectation values at the electroweak scale.
- $\mathrm{sgn}\,\mu = \pm$: the sign of the Higgsino mass term appearing in the neutralino and chargino mass matrices or in the superpotential.
- $C_{\mathrm{grav}} \geq 1$: the ratio of the gravitino mass to its value for a breaking scale Λ; it determines the lifetime of the NLSP.

The nature of the NLSP, which strongly influences the phenomenology of the scenario, depends mainly on N_5, $\tan\beta$ and Λ. For $N_5 = 1$ and small values of $\tan\beta$ the NLSP is the lightest neutralino $\widetilde{\chi}_1^0$ which decays into a photon and a gravitino [8] (p.1660). For higher values of $\tan\beta$ the $\widetilde{\tau}_1$ is the NLSP. For $N_5 \geq 2$ the NLSP is a slepton in a wide range of the parameter space as shown in Fig. 1 for the example of $N_5 = 3$. The NLSP is the $\widetilde{\tau}_1$ ($\widetilde{\ell}_R$) for large (small) values of $\tan\beta$ while for medium $\tan\beta$ values the $\widetilde{\tau}_1$ and the right-handed sleptons ($\widetilde{\mathrm{e}}_R, \widetilde{\mu}_R$) are almost degenerate in mass (*CoNLSPs*). The *CoNLSP*-region is defined as the region where the mass difference of the $\widetilde{\tau}_1$ and the right-handed sleptons ($\widetilde{\mathrm{e}}_R, \widetilde{\mu}_R$) is smaller than the tau mass. The region of small Λ and large $\tan\beta$ is theoretically excluded since it leads to tachyonic states.

In this note we study final states with τ leptons as expected for GMSB scenarios with a $\widetilde{\tau}_1$ NLSP. A typical GMSB scenario which is studied in detail in the following is given by the ATLAS benchmark scenario GMSB6 with the following parameter values: $\Lambda = 40$ TeV, $M_m = 250$ TeV, $N_5 = 3$, $\tan\beta = 30$, $\mathrm{sgn}\,\mu = +$ and $C_{\mathrm{grav}} = 1$. GMSB6 is chosen because it respects the current constraints from SM measurements as $b \to s\gamma$ and $(g_\mu - 2)/2$ and is similar to other benchmark points used in the literature, e. g. G2a [25] or SPS7 [26]. In comparison to G2a and SPS7 $\tan\beta$ is much higher to ensure that the NLSP is $\widetilde{\tau}_1$, decaying into a tau lepton and a gravitino. The mass spectrum in the GMSB6 scenario is shown in Fig. 2. Detailed numbers are given in the appendix. Apart from the quasi-massless gravitino (2.4 eV, not shown) which is the LSP, it

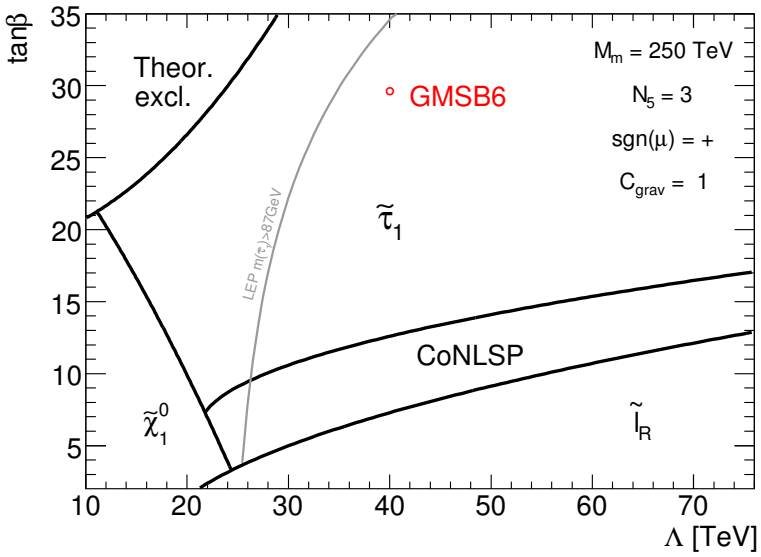

Figure 1: Nature of the NLSP in an example (Λ-tan β)-plane of the GMSB parameter space ($M_m = 250\,\text{TeV}$, $N_5 = 3$, $\text{sgn}\,\mu = +$, $C_{\text{grav}} = 1$).

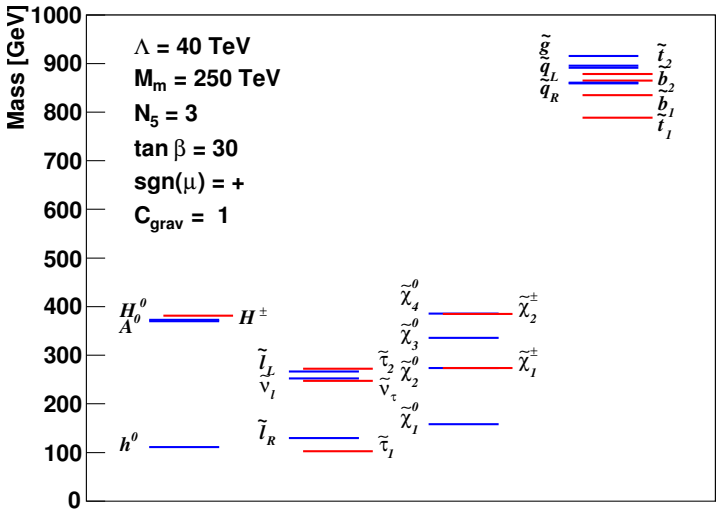

Figure 2: SUSY mass spectrum for the benchmark scenario GMSB6. The $\widetilde{\tau}_1$ (NLSP) has a mass of 102.8 GeV. The quasi-massless gravitino (2.4 eV) is not shown.

features squarks and gluinos with masses around 900 GeV, while the sleptons and gauginos have lower masses around $(100 - 400)$ GeV. The NLSP is the $\widetilde{\tau}_1$ with a mass of $m_{\widetilde{\tau}_1} = 102.8$ GeV.

In the GMSB6 scenario, the leading-order production cross section of supersymmetric particles (mainly pairs of squarks and gluinos) in pp-collisions at $\sqrt{s} = 10$ TeV (14 TeV) is given by $\sigma_{\mathrm{SUSY}} = 1.2\,\mathrm{pb}$ (3.9 pb) [27]. In R-parity conserving GMSB models which are investigated here, the initial squarks and gluinos decay through long chains into the LSP ($\widetilde{G}$) thereby producing highly energetic jets and a large amount of E_T^{miss} due to the escaping gravitino. In GMSB6 the $\widetilde{\tau}_1$ NLSP can be produced by various processes in these decay chains: 43 % (9 %) of the $\widetilde{\tau}_1$ originate from the decay of the lightest (next-to-lightest) neutralino, 28 % from the decay of right-handed sleptons and 13 % from the decay of the lightest chargino. The remaining 7% of the $\widetilde{\tau}_1$ are produced through decays of $\widetilde{\tau}_2$, $\widetilde{\chi}^0_{3,4}$, $\widetilde{\chi}^{\pm}_2$ or $\widetilde{\ell}_L$. In the GMSB6 scenario, the $\widetilde{\tau}_1$ NLSP itself always decays into a τ lepton and a gravitino. In summary, the following partial decay chains are of importance in this study as they lead to up to four τ leptons in the final state in addition to the typical signatures of high energetic jets and E_T^{miss}:

$$\begin{aligned} \widetilde{\chi}^0_{1,2} &\rightarrow \tau^{\pm}\,\widetilde{\tau}^{\mp}_1 \rightarrow \tau^{\pm}\,\tau^{\mp}\,\widetilde{G} \\ \widetilde{\ell}^{\pm}_R &\rightarrow \ell^{\pm}\,\tau^{\pm}\,\widetilde{\tau}^{\mp}_1 \rightarrow \ell^{\pm}\,\tau^{\pm}\,\tau^{\mp}\,\widetilde{G} \\ \widetilde{\chi}^{\pm}_1 &\rightarrow \nu_{\tau}\,\widetilde{\tau}^{\pm}_1 \rightarrow \nu_{\tau}\,\tau^{\pm}\,\widetilde{G}. \end{aligned} \tag{1}$$

Compared to mSUGRA models at high values of $\tan\beta$ which also lead to a $\widetilde{\tau}_1$ NLSP, GMSB models lead to a higher number of τ leptons in the final state since only the $\widetilde{\tau}_1$ can couple to the LSP in this case.

GMSB models with $\widetilde{\tau}_1$ NLSP have been searched for at LEP using the pair production of $\widetilde{\tau}_1$ and the subsequent decay $\widetilde{\tau}_1 \rightarrow \tau\widetilde{G}$. For prompt decays, $\widetilde{\tau}_1$ NLSPs with masses below 87 GeV have been excluded [28]. The corresponding region in the (Λ-$\tan\beta$)-plane is indicated in Fig. 1. The example GMSB6 scenario leads to higher $\widetilde{\tau}_1$ masses and is not excluded.

3 Event simulation

For the simulation of the GMSB signal, the SUSY mass spectrum and the branching ratios of the SUSY particles have been calculated using ISAJET 7.74 [29]. The events have been generated by HERWIG/JIMMY [27, 30, 31] including the hard scattering, the decays of SUSY particles, parton showers, hadronisation and the simulation of the underlying event. For the simulation of the response of the ATLAS detector a full GEANT4 [22, 23] simulation has been used for the example scenario, GMSB6, while for the scan in the GMSB parameter space a fast simulation approach has been adopted.

Given the total SUSY cross section of 1.2 pb the number of available fully simulated signal events for the GMSB6 scenario (9 500) corresponds to an integrated luminosity of $7.9\,\mathrm{fb}^{-1}$. For the estimation of the discovery potential, all numbers and figures are normalised to an integrated luminosity of $\mathcal{L} = 200\,\mathrm{pb}^{-1}$, whereas for the determination of the invariant mass end-point all numbers and figures are normalised to an integrated luminosity of $\mathcal{L} = 8\,\mathrm{fb}^{-1}$.

For the simulation of the SM background, the processes listed in Table 1 have been used. The datasets include di-jet and γ-jet events generated by PYTHIA 6.4 [32], W+jets and Z+jets production generated by ALPGEN [33], and di-boson, $t\bar{t}$ and single t events generated by MC@NLO [34–36]. We include higher order corrections in the form of K-factors where available: for the ALPGEN samples we apply next-to-leading order corrections, for the $t\bar{t}$ MC@NLO sample approximate next-to-next-to-leading order corrections. Again, GEANT4 has been used for the simulation of the full detector response for all SM background processes.

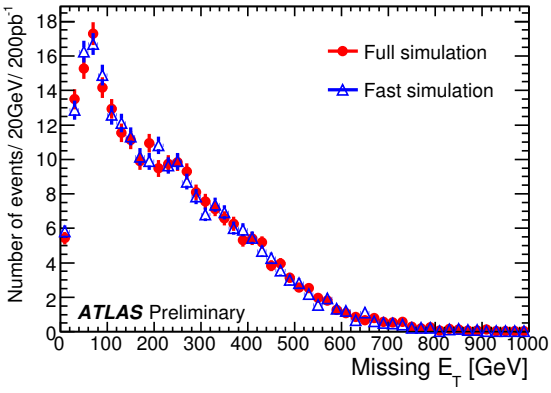

(a)

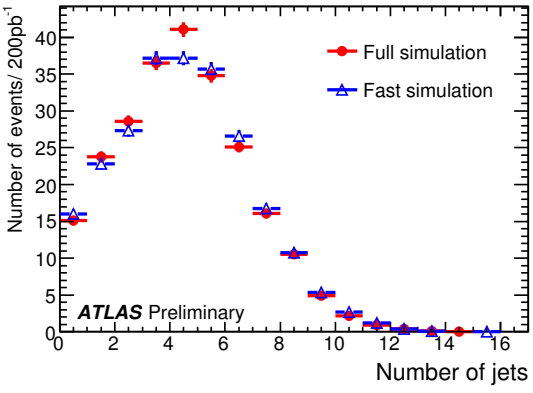

(b)

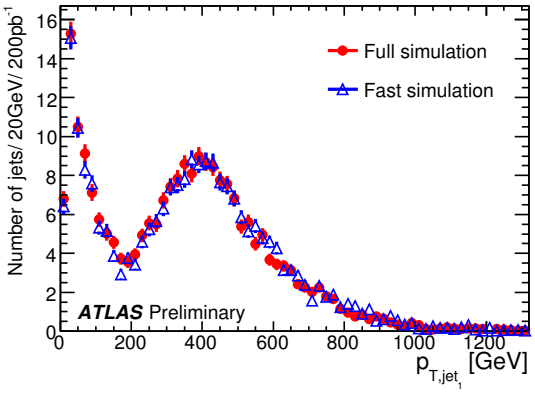

(c)

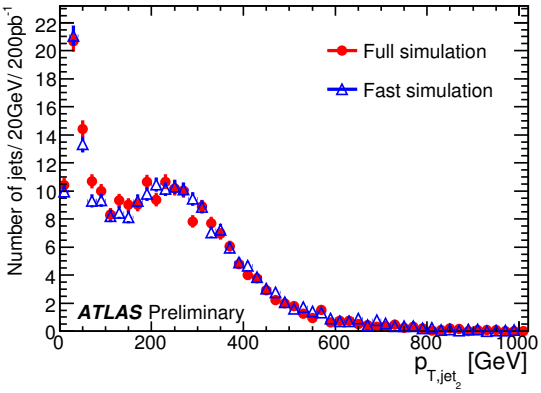

(d)

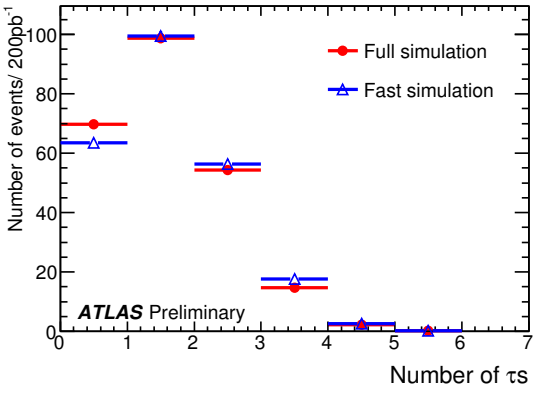

(e)

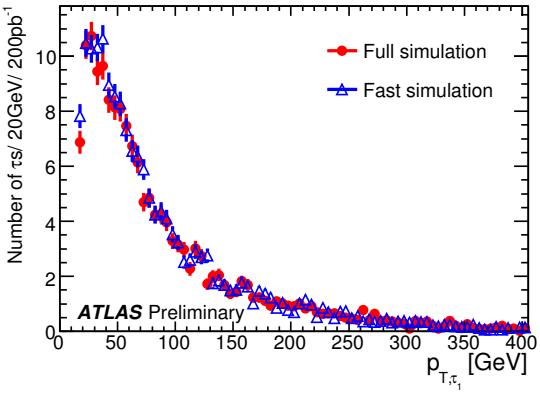

(f)

Figure 3: Comparison of the full (circles) and fast (triangles) simulation: (a) E_T^{miss}, (b) number of jets with $p_T > 20\,\text{GeV}$, (c) p_T of the leading jet, (d) p_T of the second leading jet, (e) number of τ leptons with $p_T > 15\,\text{GeV}$, (f) p_T of the leading τ lepton.

Table 1: SM background processes.

Generator	Process	cross section [pb]
MC@NLO	$t\bar{t}$	400
	single t	48
	di-boson	9.2
ALPGEN	Z+jets	$4.4 \cdot 10^3$
	W+jets	$4.8 \cdot 10^4$
Pythia	di-jet	$1.3 \cdot 10^{10}$
	γ-jet	$2.2 \cdot 10^5$

For the study of the discovery potential in the GMSB parameter space a large number of events is needed. Due to limited CPU resources we make use of a fast simulation of the ATLAS detector response [24]. A thorough comparison of the fast and full simulation results of the critical variables used in this study has been performed for the GMSB6 example scenario. Example distributions are shown in Fig. 3 for the full (circles) and fast (triangles) simulation. The observed excellent agreement of the distributions of all variables crucial for the event selection in the full and fast simulation gives confidence that the number of selected events obtained from the fast simulation reliably reproduces the results of the full simulation. Hence, the fast simulation can indeed be used in the scanning procedure.

For $M_m = 250\,\text{TeV}$, $N_5 = 3$, $\text{sgn}\,\mu = +$ and $C_{\text{grav}} = 1$ we have simulated event samples with 10 000 events each in 380 parameter points in the (Λ-$\tan\beta$)-plane, including the GMSB6 benchmark scenario. The locations of the samples in the plane have been chosen carefully to allow the investigation of the details of the phenomenology of the parameter space.

4 Study of the discovery potential

We have examined the discovery potential of ATLAS in GMSB scenarios with a $\widetilde{\tau}_1$ NLSP. The example scenario GMSB6 has been used to optimise a cut-based analysis which, in addition, has been applied in a scan of the GMSB parameter space.

4.1 Event preselection

In regions of the GMSB parameter space where the NLSP is the $\widetilde{\tau}_1$, long cascade decays of the initial squarks and gluinos lead to many highly energetic jets, many τ leptons, and a significant amount of E_T^{miss}. For this reason the following preselection is used to separate the GMSB6 signal from the SM background:

1. Events must pass the trigger selection which is optimised to select events containing at least one jet with $p_T > 70\,\text{GeV}$ and $E_T^{\text{miss}} > 30\,\text{GeV}$. This standard SUSY trigger selection is part of the ATLAS trigger menu foreseen for early data-taking [8] (p.550). The trigger efficiency for GMSB6 signal events is 80.6%. For those events which pass the preselection cuts, the trigger efficiency is 96.9%.

2. Two or more jets[1)] ($N_{\text{jets}} \geq 2$) within $|\eta| < 2.5$ have to be found, with $p_T > 100\,\text{GeV}$ for the leading jet and $p_T > 50\,\text{GeV}$ for the second-leading jet. Jet candidates also reconstructed as τ candidates have been excluded.[2)]

[1)] Jets are reconstructed from calorimeter towers using a cone algorithm with cone size of 0.4.

[2)] Two candidates are assumed to be the same if $|\Delta R| < 0.1$ with $(\Delta R)^2 = (\Delta\eta)^2 + (\Delta\phi)^2$.

Table 2: Total numbers of selected events for the signal and various SM background processes at different stages of the event selection for $\mathcal{L} = 200\,\mathrm{pb}^{-1}$ and $\sqrt{s} = 10\,\mathrm{TeV}$. The uncertainties given correspond to statistical uncertainties from the limited MC statistics. Some background processes give contributions significantly below one event after the final selection due to the selection cuts on the jet p_T and E_T^{miss} and are therefore negligible. The reason for the large rejection of dijets is because only a small fraction of such events have a sufficiently hard scatter to pass all selection requirements.

Process	Initial	Preselection	Final selection
GMSB6	240.0 ± 2.5	102.1 ± 1.6	20.4 ± 0.7
$t\bar{t}$, single t	$(8.96 \pm 0.01) \cdot 10^4$	1301 ± 11	1.1 ± 0.3
Di-boson	$(1.84 \pm 0.08) \cdot 10^3$	3.7 ± 0.4	-
Z +jets	$(8.836 \pm 0.008) \cdot 10^5$	182.1 ± 4.3	0.2 ± 0.1
W +jets	$(9.692 \pm 0.005) \cdot 10^6$	2058 ± 45	1.1 ± 1.1
Di-jet	$(2.537 \pm 0.004) \cdot 10^{12}$	$(3.5 \pm 1.7) \cdot 10^3$	-
γ-jet	$(4.40 \pm 0.01) \cdot 10^7$	20.1 ± 6.1	-

3. At least one hadronically decaying τ lepton ($N_\tau \geq 1$) with $|\eta| < 2.5$ and $p_T > 15\,\mathrm{GeV}$ has to be found with $p_T > 20\,\mathrm{GeV}$ for the leading τ. For the reconstruction of the hadronically decaying τ leptons the standard ATLAS algorithm [8] (p.230) is used. To distinguish hadronic τ decays from QCD background processes as well as from electrons and muons a number of variables offering good discrimination power are used in a combined likelihood function.[3)] Tau candidates also reconstructed as electron candidates[4)] have been excluded.[3)]

4. The missing transverse energy[5)] of the events must exceed $60\,\mathrm{GeV}$: $E_T^{\mathrm{miss}} > 60\,\mathrm{GeV}$.

5. For the removal of events with fake E_T^{miss} from mismeasured jets, the azimuthal angle between the leading jet and direction of the missing transverse energy needs to exceed 0.2: $|\Delta\phi(E_T^{\mathrm{miss}}, \text{leading jet})| > 0.2$.

Table 2 shows the total number of events from the various physics processes before and after this preselection. It can be seen that the signal-to-background ratio is greatly increased by the preselection, which retains more than 40 % of the GMSB signal events. For illustration Fig. 4(a) displays the total event numbers after each step of the preselection. The strong decrease of the background contribution is clearly visible, while the loss in signal efficiency is moderate. The strongest impact on the SM background can be observed for the trigger requirement and the requirement of at least one τ lepton. In Fig. 4(b) and Fig. 4(c) the distributions of E_T^{miss} and N_τ after the preselection are shown for the various physics processes under study. For large values of E_T^{miss} and N_τ the GMSB6 signal dominates the SM background, which mainly consists of $t\bar{t}$ and W events.

[3)] The combined likelihood is optimised for the selection of τ leptons from $Z \to \tau\tau$ decays where the dominant background consists of misidentified QCD di-jet events. Compared to a cut-based τ identification designed for first data, larger datasets are required for the study of the performance of the τ idenfication using the likelihood method as it relies on a detailed detector understanding. A cut-based identification would result in a slightly lower background rejection. A detailed study of the performance of the algorithm can be found in [8] (p.230).

[4)] Electron candidates are reconstructed and identified with the ATLAS standard *medium* purity requirements [8] (p.72). In particular, these *medium* cuts include E_T dependent isolation criteria. In addition, the electron candidate must fulfil: $p_T > 10\,\mathrm{GeV}$ and $|\eta| < 2.5$.

[5)] The value of the missing transverse energy is computed from calorimeter cells.

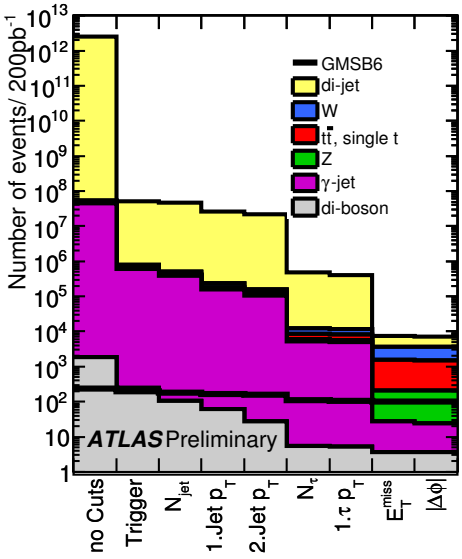

(a)

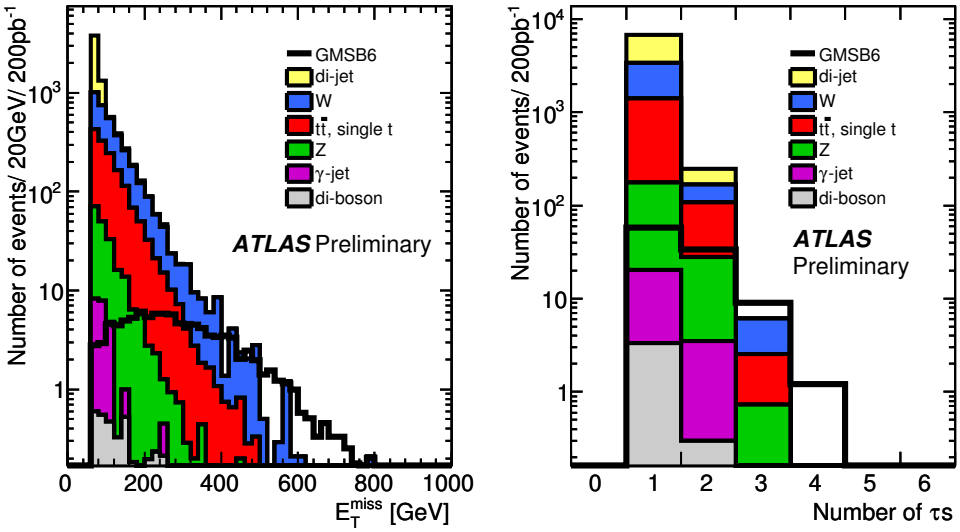

(b) (c)

Figure 4: Signal preselection: (a) total event numbers after each step of the preselection; event distributions after the preselection for the GMSB signal and the various SM backgrounds: (b) missing transverse energy, (c) number of τ leptons with $p_T > 15\,\text{GeV}$ ($p_T > 20\,\text{GeV}$ for the leading τ).

4.2 Optimisation of the final selection and signal significance for GMSB6

For further suppression of the residual SM background a two-dimensional optimisation of the signal significance as a function of the cut values of E_T^{miss} and N_τ has been performed for the GMSB6 scenario. A simplified measure for the signal significance S as a function of the cut values for the two variables is shown in Fig. 5 using the definition

$$S = N_S/\sqrt{N_B}\,, \tag{2}$$

where N_S (N_B) is the number of signal (background) events. The maximum significance can be achieved for

- $E_T^{\text{miss}} > 280\,\text{GeV}$
- $N_\tau \geq 2$.

With these two additional cuts 20.4 ± 0.7 signal events are expected for the GMSB6 scenario while the total number of expected background events is 2.5 ± 1.5 for $\mathcal{L} = 200\,\text{pb}^{-1}$. The reason for the large rejection of di-jets is because only a small fraction of such events have a sufficiently hard scatter ($p_T^{\text{leading jet}} > 100\,\text{GeV}$)) to pass the preselection cuts. This fraction is even smaller after the hard requirement on E_T^{miss} as used for the final selection. In Fig. 6(a) and Fig. 6(b) the distributions of E_T^{miss} and N_τ after the final selection excluding the cut on the displayed distribution are shown for the various physics processes under study. The resulting significance of $S = 13$ represents a promising result for searches of GMSB scenarios with a $\widetilde{\tau}_1$ NLSP with the first LHC data.

However, the simple definition of Eq. (2) neglects the influence of systematic uncertainties on the background expectation (N_B). In the real data analysis the background contribution and its uncertainty will be estimated using data-driven methods. In [8] (p.1525) the corresponding relative uncertainty, including e. g. the uncertainties from the electromagnetic and hadronic energy scale, has been conservatively estimated for electron and muon final states[6)] from Z, W and $t\bar{t}$ background processes to be 20% for a centre-of-mass energy of 14 TeV. For a smaller energy, as studied here ($\sqrt{s} = 10\,\text{TeV}$), higher uncertainties can be expected in particular for smaller datasets, as many estimates for different uncertainty sources are limited by the size of the used control sample. Taking this effect into account we assign an uncertainty of 50% for smaller datasets ($\mathcal{L} = 200\,\text{pb}^{-1}$) [37]. This relative uncertainty decreases linearly with $\mathcal{L}$ and reaches a minimum of 20% for $\mathcal{L} = 1\,\text{fb}^{-1}$. In addition, the statistical uncertainty resulting from the limited MC statistics for some MC processes enters as systematic uncertainty.

Following [38] these systematic uncertainties can be included in a more appropriate calculation of the significance Z_n using:

$$Z_n = \sqrt{2}\,\text{erf}^{-1}(1 - 2p)\,, \tag{3}$$

where erf^{-1} is the inverse error function and p is the probability that the background fluctuates to the number of measured events $N_D = N_S + N_B$, given by

$$p = A \int_0^\infty db\, G(b; N_B; \delta N_B) \sum_{i=N_D}^{\infty} \frac{e^{-b} b^i}{i!}\,, \tag{4}$$

[6)] The uncertainties on the background for τ final states, resulting for example from the performance of the τ reconstruction, in real data might be larger.

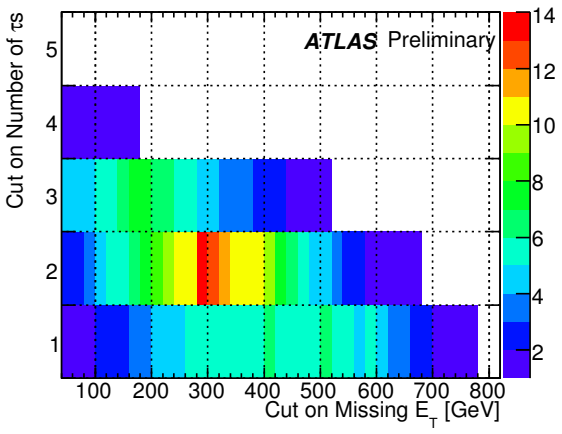

Figure 5: Signal significance ($S = N_S/\sqrt{N_B}$) as a function of the cut values of E_T^{miss} and N_τ. The maximum significance is obtained for $E_T^{\text{miss}} > 280\,\text{GeV}$ and $N_\tau \geq 2$.

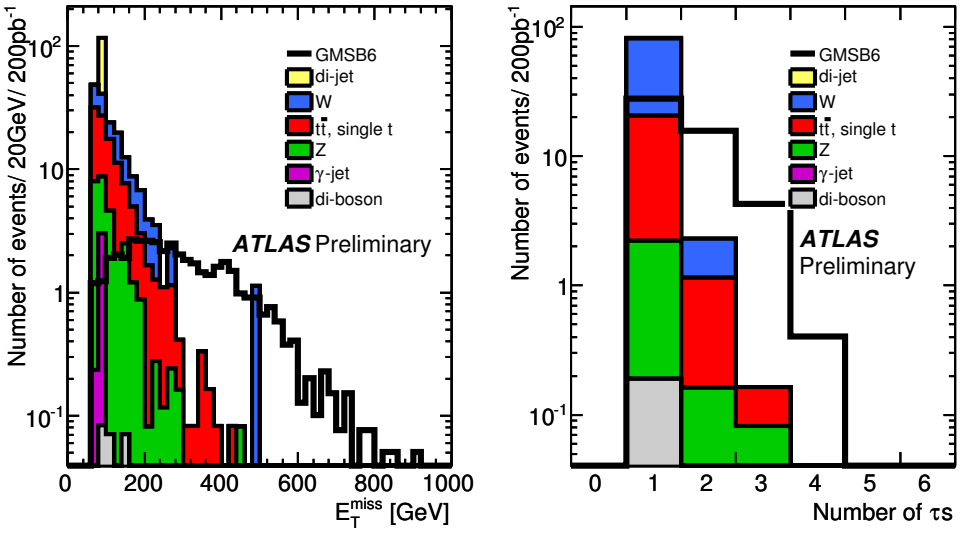

(a) (b)

Figure 6: Event distributions after the final selection for the GMSB signal and the various SM backgrounds: (a) E_T^{miss} after the $N_\tau \geq 2$ cut, (b) number of τ leptons with $p_T > 15\,\text{GeV}$ ($p_T > 20\,\text{GeV}$ for the leading τ) after the $E_T^{\text{miss}} > 280\,\text{GeV}$ cut.

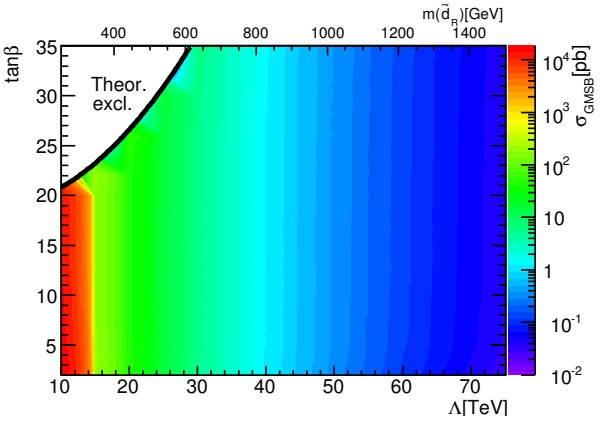

Figure 7: Total SUSY cross section in pb at $\sqrt{s} = 10\,\text{TeV}$ in the (Λ-tan β)-plane for $M_m = 250\,\text{TeV}$, $N_5 = 3$, sgn $\mu = +$ and $C_{\text{grav}} = 1$. It strongly depends on Λ due to the increase of the masses of the SUSY particles with increasing Λ.

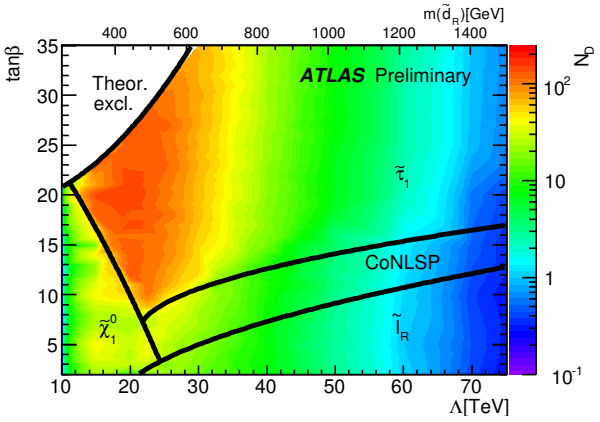

Figure 8: Expected number of selected signal events for $\mathcal{L} = 200\,\text{pb}^{-1}$ in the (Λ-tan β)-plane for $M_m = 250\,\text{TeV}$, $N_5 = 3$, sgn $\mu = +$ and $C_{\text{grav}} = 1$. The expected number of corresponding background events is $N_B = 2.5$.

where $G(b; N_B; \delta N_B)$ is a Gaussian distribution and A is the normalisation factor given by

$$A^{-1} = \int_0^\infty db\, G(b; N_B; \delta N_B) \sum_{i=0}^{\infty} \frac{e^{-b} b^i}{i!}\,. \tag{5}$$

In general, this approach provides a more conservative estimate of the signal significance than using Eq. (2), e. g. for the GMSB6 scenario we obtain a reduced signal significance of $Z_n = 5.7$. The two-dimensional optimisation procedure using the significance definition of Eq. (3) yields the same optimal selection cuts for E_T^{miss} and N_τ as before using Eq. (2).

4.3 Scan of the GMSB parameter space

As mentioned above, a scan of the parameter space can only be done with fast simulation samples (see Sec. 3). Since the comparison of the individual variables in the full and fast simulation demonstrated in general a good agreement only small differences in the total number of events after the application of the selection are expected.

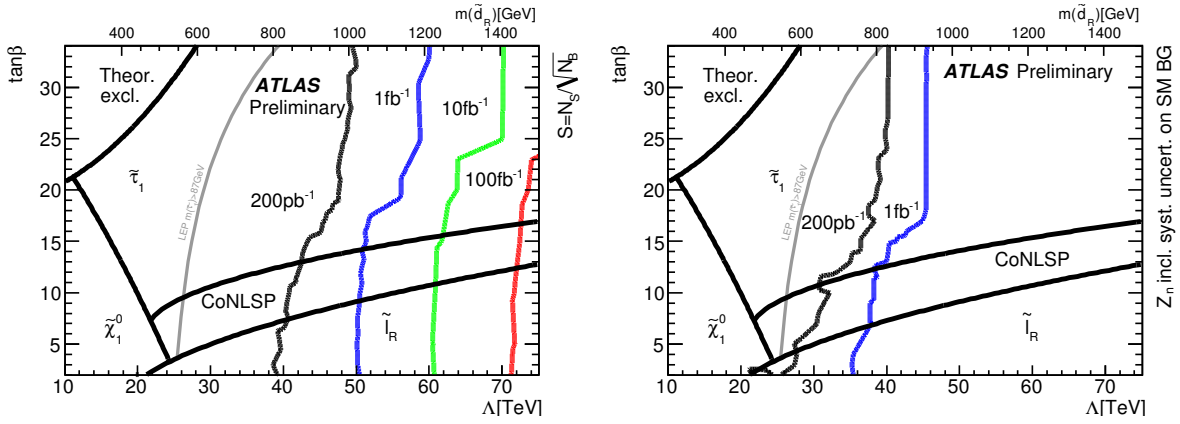

(a) (b)

Figure 9: Integrated luminosity needed for a signal significance of $S = 5$ or $Z_n = 5$, respectively, in the (Λ-$\tan\beta$)-plane for $M_m = 250\,\text{TeV}$, $N_5 = 3$, $\text{sgn}\,\mu = +$ and $C_{\text{grav}} = 1$ using (a) the simple calculation of the significance following Eq. (2) which neglects the uncertainty on the SM background and (b) using Eq. (3) which properly includes this uncertainty.

We study the discovery potential in the (Λ-$\tan\beta$)-plane for $M_m = 250\,\text{TeV}$, $N_5 = 3$, $\text{sgn}\,\mu = +$ and $C_{\text{grav}} = 1$. Out of the six GMSB model parameters Λ and $\tan\beta$ have the strongest influence on the event topology. These parameter values restrict the analysis to specific NLSPs and final states (see Sec. 2) and to promptly decaying NLSPs. Figure 7 shows the total SUSY production cross section in the studied plane. While only a small dependence on the cross section on $\tan\beta$ can be observed, the cross section strongly depends on Λ due to the increase of the masses of the SUSY particles with increasing Λ. For example, in the range $\Lambda = 10\,\text{TeV}$ to $\Lambda = 50\,\text{TeV}$ the cross section falls by four orders of magnitude. This decrease of the cross section is reflected in the values of the total number of selected signal events[7)] which are displayed in Fig. 8 for $200\,\text{pb}^{-1}$. In addition to the decrease of the production cross section with Λ, the nature of the NLSP has a strong influence on the number of selected events. While the regions with a $\widetilde{\tau}_1$ NLSP feature a large fraction of selected events, selection losses can be observed in regions where the NLSP is given by $\widetilde{\ell}_R$, $\widetilde{\chi}_1^0$ or in the CoNLSP region due to the dominant final states with electrons, muons or photons for which the selection is not optimised.

The number of selected signal events in the (Λ-$\tan\beta$)-plane for $200\,\text{pb}^{-1}$ (Fig. 8) and the expected number of background events from the full simulation study (see Sec. 4.1) can be translated into a signal significance as a function of the integrated luminosity $\mathcal{L}$ using the definitions in Eq. (2) or Eq. (3) and an appropriate scaling with $\mathcal{L}$. The corresponding results are shown in Fig. 9(a) using Eq. (2) for the calculation of the signal significance which neglects the systematic uncertainties of the background. As expected, the values of $\mathcal{L}$ needed for $S = 5$ are small in regions with a $\widetilde{\tau}_1$ NLSP and small/medium values of Λ. With a luminosity of only $\mathcal{L} = 200\,\text{pb}^{-1}$, expected to be available after one year of data-taking, $S = 5$ can be reached in the parameter space region up to $\Lambda \sim 45\,\text{TeV}$. Due to the strong reduction of the cross section the signal significance strongly decreases with increasing Λ leading to $S = 5$ regions up to $\Lambda \sim 60\,\text{TeV}$ ($\Lambda \sim 70\,\text{TeV}$) for $\mathcal{L} = 1\,\text{fb}^{-1}$ ($\mathcal{L} = 10\,\text{fb}^{-1}$).

However, the inclusion of the background uncertainty in the calculation of the signal signif-

[7)] The same selection as presented in Sec. 4.1 and 4.2 has been applied.

icance following Eq. (3) leads to more conservative results as displayed in Fig. 9(b). With this definition the parameter region for a 5σ discovery with $\mathcal{L} = 200\,\mathrm{pb}^{-1}$ ($1\,\mathrm{fb}^{-1}$) is reduced to the region up to $\Lambda \sim 40\,\mathrm{TeV}$ (45 TeV). With the current assumptions on the background uncertainty of 20% for data samples of $1\,\mathrm{fb}^{-1}$ or higher the discovery reach can not be improved. However, the contributions to the background uncertainty, which are limited by the size of the used control samples, will gain directly from a larger data sample and therefore decrease. Further, an improved understanding of the backgrounds and their uncertainties is expected from dedicated studies by the time larger datasets of real τ leptons expected from SM processes are available.

5 Study of the invariant di-tau mass distribution

After a possible SUSY discovery the investigation of the underlying SUSY model is an important step in which the determination of the masses of SUSY particles is vital. In the presence of two undetected LSPs only differences of SUSY masses can be determined at the LHC, e. g. from kinematic end-points in invariant mass distributions. While in the past only few studies in this area have been performed for GMSB scenarios, extensive results are available for mSUGRA-like scenarios [8] (p.1617). For example the end-point of the reconstructed di-tau invariant mass has been used to determine the underlying masses in the mSUGRA SU3 scenario in which the lightest neutralino ($\widetilde{\tau}_1$) is the LSP (NLSP) yielding the decay chain $\widetilde{\chi}_2^0 \to \widetilde{\tau}_1\,\tau \to \widetilde{\chi}_1^0\,\tau\,\tau$. In the following we study the application of the techniques developed in the aforementioned scenario to our GMSB6 model in which we expect slightly different kinematics (due to the massless gravitino) and additional background from other SUSY decays ($\widetilde{\ell}_R$, $\widetilde{\chi}_2^0$).

For the study of the kinematic end-point of the invariant mass of two τ leptons we consider larger datasets ($8\,\mathrm{fb}^{-1}$) and we loosen the final selection criteria of Sec. 4.1 in order to allow for a sufficient event statistics which is needed for the following measurement and the estimation technique for the SM contribution. This study of the invariant mass of two τ leptons will not be possible with early data ($200\,\mathrm{pb}^{-1}$). Although, given the number of selected events and the expected result on the kinematic endpoint of the invariant mass distribution as discussed in this Section, we might be able to glimpse at the invariant mass distribution already with medium-size datasets of $1\,\mathrm{fb}^{-1}$.

The selection includes the standard preselection cuts and in addition the following requirements

$$N_\tau \geq 2 \qquad \text{and} \qquad \left(\frac{E_T^{\mathrm{miss}}}{300\,\mathrm{GeV}}\right)^2 + \left(\frac{p_{T,\mathrm{leading\,jet}}}{600\,\mathrm{GeV}}\right)^2 > 1. \tag{6}$$

We show the number of events in the (E_T^{miss}-$p_{T,\mathrm{leading\,jet}}$)-plane for the signal in Fig. 10(a) and for the background in Fig. 10(b). They illustrate an efficient background suppression while keeping a good signal fraction. With this relaxed final selection $29.2 \pm 0.9\,(1169 \pm 5)$ signal events are expected for the GMSB6 scenario while the total number of expected background events is $6.1 \pm 2.3\,(244 \pm 14)$ for $\mathcal{L} = 200\,\mathrm{pb}^{-1}\,(8\,\mathrm{fb}^{-1})$.

For selected signal events the distribution of the di-tau invariant mass $m_{\tau\tau}$ at generator level is shown in Fig. 11(a). As expected from Eq. (1) the distribution consists of three contributions: decays of the two lightest neutralinos and decays of either right-handed selectrons or smuons. Other contributions, e. g. from the $\widetilde{\chi}_1^\pm$ decay, are negligible. The contributions from neutralino decays feature the typical triangular shape including the edge at the theoretically expected end-points (120.1 GeV, 253.3 GeV). The distribution from slepton decays has, however, no sharp triangular end-point due to the additional lepton arising in the decay which is not included in the mass calculation. For this reason the distribution is smeared out still offering the theoretical end-point of 79.2 GeV.

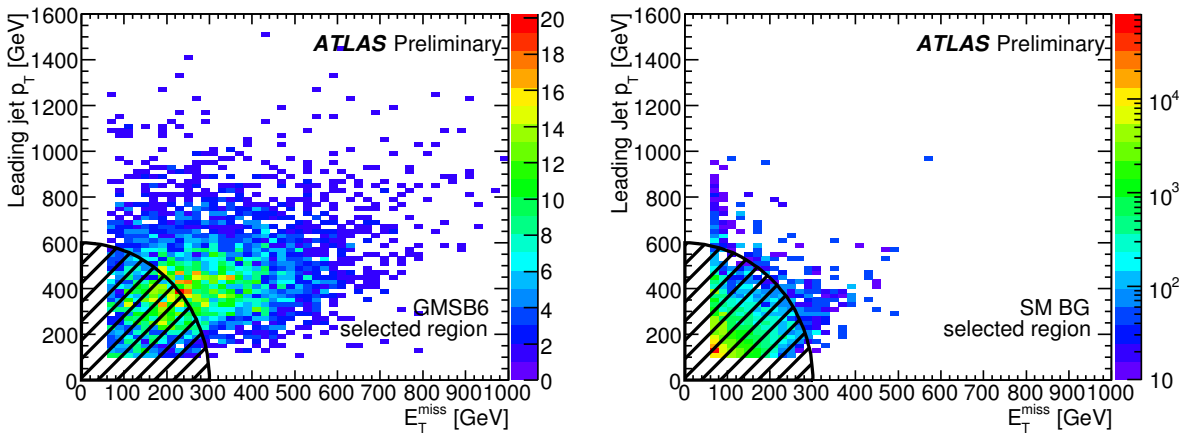

(a) (b)

Figure 10: Distribution of events in the plane of E_T^{miss} and p_T of the leading jet for (a) the signal and (b) the SM background for $8\,\text{fb}^{-1}$. The elliptical cut is indicated by the hashed region. All events outside this region are selected.

The corresponding $m_{\tau\tau}$ distributions at reconstruction level, calculated from the visible decay products of the tau pair, are shown in Fig. 11(b) assuming the correct combination of the final state τ leptons using MC information. Due to the unmeasured neutrinos in the τ decays the characteristic kinematic end-point of the $\widetilde{\chi}_1^0$ decays is lost and the direct extraction of the end-point is impeded. In addition it can be seen that only a small fraction of the τ leptons from $\widetilde{\ell}_R$ decays are reconstructed and as a result the $\widetilde{\ell}_R$ contribution is small. The reason is the additional lepton in the slepton decay which is often located inside the τ reconstruction cone due to the small mass difference between $\widetilde{\tau}_1$ and the slepton (Fig. 2). The additional lepton inside the cone leads to differences in the distributions of the individual variables used for the construction of the likelihood and consequently to a smaller acceptance. In addition, τ leptons from slepton decays yield smaller values of p_T leading to a further reduction of the reconstruction efficiency due to the $p_T > 15\,\text{GeV}$ requirement.

In the real experiment the correct combination and origin of the final state τ leptons is unknown and all possible combinations must be considered. The resulting invariant mass distribution is shown in Fig. 12(a) for the GMSB6 signal and the various SM background processes.[8)] It can be seen that the overall contribution from SM background is small. Here, different combinations of true and fake tau leptons are possible, although the main contribution comes from the combination of one true and one fake tau lepton as from W boson or $t\bar{t}$ production. Large contributions from Z bosons are not seen, as some E_T^{miss} is required by the event selection. Besides the contribution from fake tau leptons the GMSB signal contains up to four tau leptons, leading to a large number of wrong combinations. The contribution of di-tau pairs from wrong combinations can be corrected by a subtraction of the $m_{\tau\tau}$ distribution of two τ leptons with the same measured charge from the distribution with opposite charge (OS-SS), assuming that wrong di-tau combinations contribute equally to the OS and SS distributions. The corre-

[8)] Only two of the generated MC events of the W production fulfil the selection criteria. They would enter the invariant mass distribution with high event weights. Instead we use the shape of the W contribution determined with a looser selection and scale it accordingly.

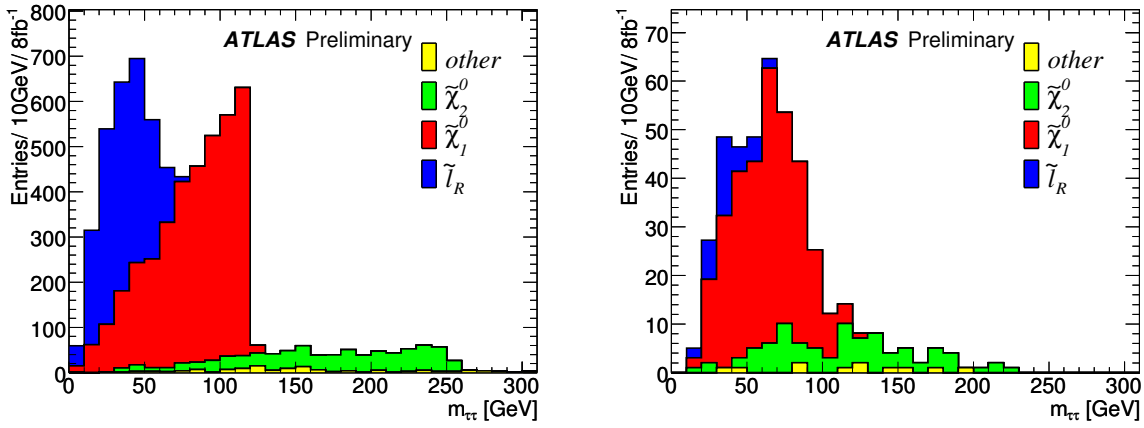

(a) (b)

Figure 11: Invariant mass distribution of two τ leptons originating from different decay processes for the GMSB6 signal: (a) generator level, (b) reconstruction level for selected events.

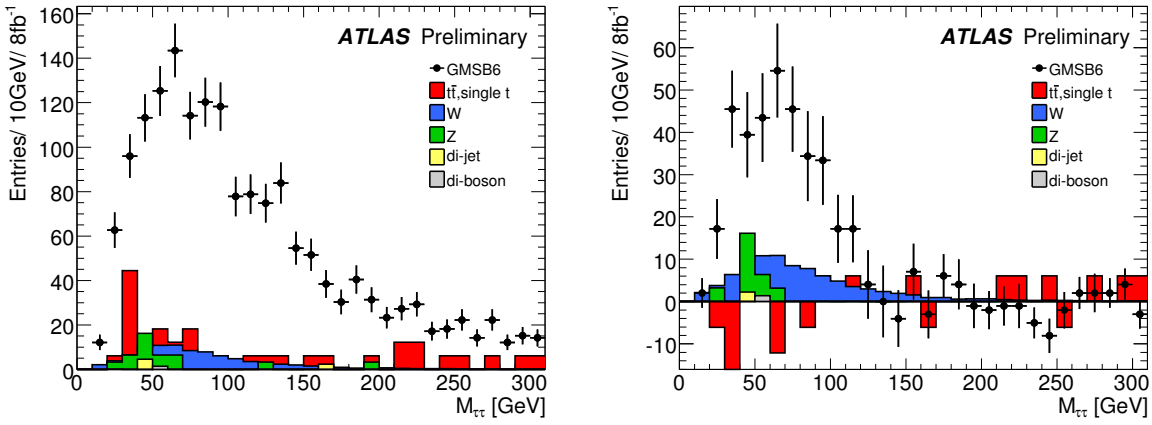

(a) (b)

Figure 12: Invariant mass distribution of (a) any two τ leptons for the GMSB6 signal and the SM background after the selection and (b) the same-sign distribution (SS) subtracted from the opposite-sign distribution (OS) for $\mathcal{L} = 8\,\mathrm{fb}^{-1}$.

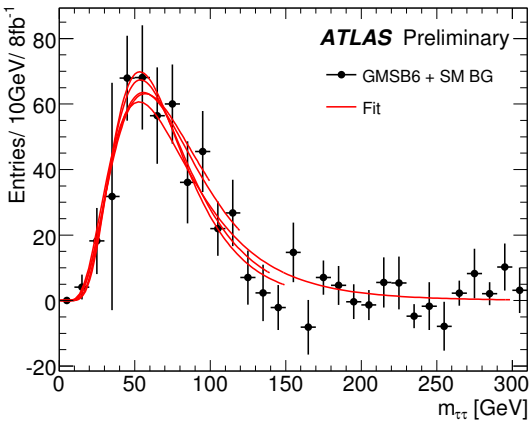

Figure 13: Example fits of the invariant mass (OS-SS) distribution using different fit ranges.

sponding distributions are shown in Fig. 12(b) for the GMSB6 signal and the SM background processes. The distribution for the GMSB6 signal shows nice agreement with the corresponding distribution using generator information for the assignment (Fig. 11(b)).

Applying the procedure proposed for the clean SU3 scenario [8] (p.1617) the combined OS-SS distribution can be fitted using an appropriate function[9)] to extract the inflection point of the distribution $M_{\tau\tau}^{\mathrm{IP}}$ which can be directly translated into the kinematic end-point $m_{\tau\tau}^{\mathrm{max}}$ using a linear calibration curve. The calibration curve is determined from fast simulation results of 14 SU3-like models with varying $\widetilde{\tau}_1$ and neutralino masses as $M_{\tau\tau}^{\mathrm{IP}} = (0.47 \pm 0.02) m_{\tau\tau}^{\mathrm{max}} + (15 \pm 2)\mathrm{GeV}$. The covariance between the slope and the intercept of the calibration function has been determined as $-0.034\,\mathrm{GeV}$.

Using this method we obtain for the GMSB6 scenario an inflection point of $M_{\tau\tau}^{\mathrm{IP}} = (78.4 \pm 2.0)\,\mathrm{GeV}$ which results in a kinematic end-point of $m_{\tau\tau}^{\mathrm{max}} = (135.0 \pm 4.3)$ GeV, where the error given specifies the uncertainty from the fit only. The determination of the kinematic end-point as detailed above is subject to several sources of systematic uncertainty:

- **Uncertainty from varying fit ranges:** We have repeated the fits to the $m_{\tau\tau}$ spectrum using various fit ranges as detailed in Fig. 13. We obtain $\sigma^{\mathrm{fit\,range}} = ^{+10}_{-4}$ GeV.

- **Uncertainty from the initial calibration curve:** The calibration curve for the translation of the deflection point into an end-point measurement has an uncertainty. Taking into account the uncertainty and the correlations results in an additional systematic uncertainty of $\sigma^{\mathrm{calib}} = \pm 2.7\,\mathrm{GeV}$.

- **Uncertainty from tau polarisation:** Parity violation in weak interactions in conjunction with momentum and angular momentum conservation leads to a correlation between the visible tau energy and the polarisation of the tau. Hence the di-tau invariant mass distribution has a dependence on the tau polarisation. Within the GMSB model the tau polarisation is known for the different SUSY particles decaying into a tau. Nevertheless the relative composition of different decays can change. We assign a systematic uncertainty of $\sigma^{\mathrm{pol}} = \pm 7.0\,\mathrm{GeV}$ due to variations in the tau polarisation [8] (p.1628).

[9)] The used function was optimised for the clean SU3 scenario and does not reflect the additional contribution $(\widetilde{\ell}_R, \widetilde{\chi}_2^0)$ present in GMSB scenarios.

- **Uncertainty from SM background contributions:** We use the OS-SS di-tau invariant mass distribution to remove wrong di-tau combinations from our sample. With this technique most of the SM background is removed. As can be seen in Fig. 12(b) the SM background is not zero on average and hence some residual dependence from the SM background on the measured kinematic end-point is expected. As mentioned above the uncertainty on the background estimation is assumed to be around 20%. For an estimation of the related uncertainty on the final result we multiply the background by factors of 1.2 and 0.8 and determined the deviations of $m_{\tau\tau}^{\max}$ from the central result. In order to account for possible differences in the shape or normalisation between OS and SS distributions, we vary the background separately for OS and SS. We obtain $\sigma^{\mathrm{SM\,BG}} = ^{+1.9}_{-2.3}$ GeV.

Adding these systematic uncertainties and the statistical uncertainty resulting from the fit in quadrature we obtain $m_{\tau\tau}^{\max} = \left(135^{+13}_{-10}\right)$ GeV for our measurement. A slight overestimation ($1.5\,\sigma$) of the reconstructed end-point compared to the expected value of 120 GeV can be observed. This overestimation is a result of the additional SUSY background contribution from $\widetilde{\chi}_2^0$ and $\widetilde{\ell}_R$ decays which has not been taken into account in the fit function which was constructed for the background-free SU3 case. Due to the small statistics available and the unknown underlying true distribution of each contribution a simultaneous fit of all contributions was found to be very challenging for $\mathcal{L} = 8\,\mathrm{fb}^{-1}$. In a real measurement other decay chains might be used to additionally constrain these contributions from other SUSY processes. Since the $\widetilde{\chi}_2^0$ background is mainly located at high values of $m_{\tau\tau}$ a slight bias of the method is expected. On the other hand the $\widetilde{\ell}_R$ background is located at low values of $m_{\tau\tau}$ which could partly compensate the effect from the $\widetilde{\chi}_2^0$ decays.

The impact of the additional SUSY background strongly depends on the unknown SUSY model realised in nature. For a more detailed study of this effect on our method the $m_{\tau\tau}$ fit has been repeated for the GMSB6 example scenario on truth matched[10] τ candidates excluding or doubling those from the $\widetilde{\chi}_2^0$ or $\widetilde{\ell}_R$ decays. We observed a shift of the final result of ± 13 GeV. This range gives an indication of the additional systematic uncertainty resulting from additional SUSY background which must be taken into account. In addition we studied samples of fast simulations at various points in the GMSB parameter space and found in general a much smaller bias towards larger values (always within $1\,\sigma$).

Including the contribution from SUSY background as an additional systematic uncertainty, we obtain:

$$m_{\tau\tau}^{\max} = \left(\, 135 \pm 4\,(\mathrm{stat.})\, ^{+13}_{-9}\,(\mathrm{sys.})\, \pm 13\,(\mathrm{SUSY\,model})\,\right)\ \mathrm{GeV}\,. \tag{7}$$

The results obtained in this chapter demonstrate that a measurement of the end-point of the invariant di-tau mass spectrum might be possible in the GMSB6 example scenario with a small bias from additional SUSY background. The determined value can then be used to constrain the space of the underlying parameters of the GMSB model, maybe in combination with other experimental results in a global fit of the GMSB model which is beyond the scope of this note.

6 Summary and conclusion

In this note we have studied the expected performance of the ATLAS detector in GMSB SUSY models with a $\widetilde{\tau}_1$ NLSP leading to final states with large missing transverse energy, highly energetic jets and up to four τ leptons. It has been demonstrated that a discovery of GMSB

[10] A reconstructed τ candidate is called truth matched if a τ lepton at generator level is found in a cone of $\Delta R < 0.1$ around the candidate.

models with a $\widetilde{\tau}_1$ NLSP is possible in large parts of the supersymmetric parameter space using a cut-based analysis. After a possible discovery a determination of the end-point in the invariant di-tau mass is possible with larger datasets and small bias in these scenarios.

A Appendix

A.1 GMSB6 mass spectrum

Table 3: Detailed mass spectrum for the GMSB6 benchmark point. All masses are in GeV. The quasi-massless gravitino (2.4 eV) is not listed.

$\widetilde{\mathrm{g}}$	915.3	$\widetilde{\chi}_1^0$	158.0	$\widetilde{\nu}_e$	252.4	h	110.9
$\widetilde{\mathrm{u}}_L$	891.6	$\widetilde{\chi}_2^0$	273.4	$\widetilde{\mathrm{e}}_L$	266.8	H	372.5
$\widetilde{\mathrm{u}}_R$	860.9	$\widetilde{\chi}_3^0$	335.7	$\widetilde{\mathrm{e}}_R$	129.8	A	370.1
$\widetilde{\mathrm{d}}_L$	895.5	$\widetilde{\chi}_4^0$	385.9	$\widetilde{\nu}_\tau$	247.5	$\mathrm{H}^\pm$	381.6
$\widetilde{\mathrm{d}}_R$	859.3	$\widetilde{\chi}_1^\pm$	273.8	$\widetilde{\tau}_1$	102.8		
$\widetilde{\mathrm{b}}_1$	834.8	$\widetilde{\chi}_2^\pm$	384.6	$\widetilde{\tau}_2$	272.1		
$\widetilde{\mathrm{b}}_2$	865.2						
$\widetilde{\mathrm{t}}_1$	788.3						
$\widetilde{\mathrm{t}}_2$	878.5						

References

[1] ATLAS Collaboration, G. Aad et al., *The ATLAS experiment at the CERN Large Hadron Collider*, JINST **3** (2008) S08003.

[2] CMS Collaboration, R. Adolphi et al., *The CMS experiment at the CERN LHC*, JINST **3** (2008) S08004.

[3] L. Evans, (ed.) and P. Bryant, (ed.), *LHC Machine*, JINST **3** (2008) S08001.

[4] H. Nilles, *Supersymmetry, supergravity and particle physics*, Phys. Rept. **110** (1984) 1.

[5] H. E. Haber and G. L. Kane, *The search for supersymmetry: Probing physics beyond the Standard Model*, Phys. Rept. **117** (1985) 75.

[6] J. Wess and J. Bagger, *Supersymmetry and supergravity*. Univ. Pr. Princeton, 1992.

[7] S. Martin, *A supersymmetry primer*, `hep-ph/9709356`.

[8] The ATLAS Collaboration, G. Aad et al., *Expected performance of the ATLAS experiment - Detector, trigger and physics*, `CERN-OPEN-2008-020`.

[9] CMS Collaboration, G. L. Bayatian et al., *CMS technical design report, volume II: Physics performance*, J. Phys. **G34** (2007) 995–1579.

[10] L. Alvarez-Gaume, J. Polchinski, and M. Wise, *Minimal low-energy supergravity*, Nucl. Phys. **B221** (1983) 495.

[11] L. Ibanez, *Locally supersymmetric SU(5) grand unification*, Phys. Lett. **B118** (1982) 73.

[12] J. Ellis, D. Nanopoulos, and K. Tamvakis, *Grand unification in simple supergravity*, Phys. Lett. **B121** (1983) 123.

[13] K. Inoue, A. Kakuto, H. Komatsu, and S. Takeshita, *Aspects of grand unified models with softly broken supersymmetry*, Prog. Theor. Phys. **68** (1982) 927.

[14] A. Chamseddine, R. Arnowitt, and P. Nath, *Locally supersymmetric grand unification*, Phys. Rev. Lett. **49** (1982) 970.

[15] L. Alvarez-Gaume, M. Claudson, and M. Wise, *Low-energy supersymmetry*, Nucl. Phys. **B207** (1982) 96.

[16] M. Dine, W. Fischler, and M. Srednicki, *Supersymmetric technicolor*, Nucl. Phys. **B189** (1981) 575.

[17] S. Dimopoulos and S. Raby, *Supercolor*, Nucl. Phys. **B192** (1981) 353.

[18] C. R. Nappi and B. A. Ovrut, *Supersymmetric extension of the SU(3)×SU(2)×U(1) Model*, Phys. Lett. **B113** (1982) 175.

[19] M. Dine and A. Nelson, *Dynamical supersymmetry breaking at low-energies*, Phys. Rev. **D48** (1993) 1277, `hep-ph/9303230`.

[20] M. Dine, A. Nelson, and Y. Shirman, *Low-energy dynamical supersymmetry breaking simplified*, Phys. Rev. **D51** (1995) 1362, `hep-ph/9408384`.

[21] M. Dine, A. Nelson, Y.Nir, and Y. Shirman, *New tools for low-energy dynamical supersymmetry breaking*, Phys. Rev. **D53** (1996) 2658, `hep-ph/9507378`.

[22] GEANT4 Collaboration, S. Agostinelli et al., *GEANT4: A simulation toolkit*, Nucl. Instrum. Meth. **A506** (2003) 250.

[23] J. Allison et al., *Geant4 developments and applications*, IEEE Trans. Nucl. Sci. **53** (2006) 270.

[24] K. Assamagan et al., *The ATLAS simulation project*, To be submitted to JINST, 2009.

[25] I. Hinchliffe and F. E. Paige, *Measurements in gauge mediated SUSY breaking models at LHC*, Phys. Rev. **D60** (1999) 095002, `arXiv:hep-ph/9812233`.

[26] B. C. Allanach et al., *The Snowmass points and slopes: Benchmarks for SUSY searches*, Eur. Phys. J. **C25** (2002) 113–123, `arXiv:hep-ph/0202233`.

[27] G. Corcella et al., *HERWIG 6.5: an event generator for Hadron Emission Reactions With Interfering Gluons (including supersymmetric processes)*, JHEP **01** (2001) 010, `arXiv:hep-ph/0011363`.

[28] LEPSUSYWG, ALEPH, DELPHI, L3 and OPAL Experiments, *Combined LEP GMSB stau/smuon/selectron results, 189-208 GeV*, 2002. LEPSUSYWG/02-09.2.

[29] F. E. Paige, S. D. Protopopescu, H. Baer, and X. Tata, *ISAJET 7.69: A Monte Carlo event generator for pp, $\bar{p}p$, and e^+e^- reactions*, `arXiv:hep-ph/0312045`.

[30] G. Corcella et al., *HERWIG 6.5 release note*, `arXiv:hep-ph/0210213`.

[31] J. M. Butterworth, J. R. Forshaw, and M. H. Seymour, *Multiparton interactions in photoproduction at HERA*, Z. Phys. **C72** (1996) 637–646, arXiv:hep-ph/9601371.

[32] T. Sjöstrand, S. Mrenna, and P. Skands, *PYTHIA 6.4 physics and manual*, JHEP **05** (2006) 026, arXiv:hep-ph/0603175.

[33] M. L. Mangano, M. Moretti, F. Piccinini, R. Pittau, and A. D. Polosa, *ALPGEN, a generator for hard multiparton processes in hadronic collisions*, JHEP **07** (2003) 001, arXiv:hep-ph/0206293.

[34] S. Frixione and B. R. Webber, *Matching NLO QCD computations and parton shower simulations*, JHEP **06** (2002) 029, arXiv:hep-ph/0204244.

[35] S. Frixione, P. Nason, and B. R. Webber, *Matching NLO QCD and parton showers in heavy flavour production*, JHEP **08** (2003) 007, arXiv:hep-ph/0305252.

[36] S. Frixione, E. Laenen, P. Motylinski, and B. R. Webber, *Single-top production in MC@NLO*, JHEP **03** (2006) 092, arXiv:hep-ph/0512250.

[37] ATLAS Collaboration, *Prospects for SUSY and UED discovery based on inclusive searches at a 10 TeV centre-of-mass energy with the ATLAS detector*, ATL-PHYS-PUB-2009-084, 2009.

[38] J. T. Linnemann, *Measures of significance in HEP and astrophysics*, arXiv:physics/0312059. Published in proceedings of PHYSTAT2003: *Statistical problems in particle physics, astrophysics, and cosmology*, Menlo Park, California, 2003.